Relative contribution of temperature and salinity to ocean acoustic reflectivity

V. Sallarès,[1] B. Biescas,[1] G. Buffett,[2] R. Carbonell,[2] J. J. Dañobeitia,[1] and J. L. Pelegrí[3]

Received 22 July 2009; revised 2 September 2009; accepted 23 September 2009; published 23 October 2009.

[1] Marine seismic data display laterally coherent reflectivity from the water column that is attributed to fine-scale oceanic layering. The amplitude of the different reflections is the expression of acoustic impedance contrasts between neighbouring water masses, and therefore water reflectivity maps the ocean's vertical sound speed and density (i.e., temperature and salinity) variations. Here we determine the relative contribution of each parameter by computing the temperature and salinity partial derivatives of sound speed and density, and using them to estimate reflection coefficients from a real oceanographic dataset. The results show that the mean contribution of density variations is 5–10%, while 90–95% is due to sound speed variations. On average, 80% of reflectivity comes from temperature contrasts. Salinity contribution averages 20%, but it is highly variable and reaches up to 40% in regions prone to diffusive convection such as the top of the Mediterranean Undercurrent in the Gulf of Cadiz. **Citation:** Sallarès, V., B. Biescas, G. Buffett, R. Carbonell, J. J. Dañobeitia, and J. L. Pelegrí (2009), Relative contribution of temperature and salinity to ocean acoustic reflectivity, *Geophys. Res. Lett.*, *36*, L00D06, doi:10.1029/2009GL040187.

1. Introduction

[2] Multichannel seismics (MCS) is a widely used tool for geological prospection of the Earth's subsurface. Marine MCS systems are constituted of a source, generally an airgun array, and a line of closely spaced hydrophones, or channels, called a streamer that are towed behind a vessel. The airguns are fired at constant intervals, the seismic wavefield propagates through the medium, scatters back, and is recorded by the streamer. The seismograms recorded in the different channels are then ordered, processed and stacked to generate laterally coherent images of the different reflecting discontinuities, whose amplitude is proportional to the impedance (sound speed × density) contrast across the discontinuity. The basic "convolutional model" for seismic reflection data shows that seismic traces can be interpreted as the convolution of the source wavelet with the medium's elementary reflection coefficients [e.g., *Sheriff and Geldart*, 1995]. The vertical resolution of the seismic data depends therefore on the source used, and its capacity to distinguish between two adjoining layers is given by the Rayleigh criterion of a quarter of the dominant wavelength [*Widess*, 1973].

[3] *Holbrook et al.* [2003] showed that marine MCS data display reflectivity not only from solid Earth interfaces but also from within the water column. Practically, this indicates that the seismic systems are sensitive to the vertical sound speed and/or density variations of the ocean's interior. This observation has in the recent years given rise to a number of studies showing seismic images of water mass fronts and currents [e.g., *Tsuji et al.*, 2005], and mesoscale features such as Meddies [*Biescas et al.*, 2008] or the Mediterranean Undercurrent [*Buffett et al.*, 2009]. The central frequency of the seismic sources used in most of these experiments range between ∼20 Hz and ∼100 Hz, so its effective vertical resolution is on the order of ∼10 m. This is the approximate vertical dimension of oceanic fine structure, present in most of the world's oceans and whose origin has been attributed to a variety of physical phenomena such as double-diffusion [e.g., *Ruddick and Gargett*, 2003]. In parallel, it has been shown that there is a good correlation between ocean's reflectivity and vertical temperature gradient [*Nandi et al.*, 2004; *Nakamura et al.*, 2006], and that wave number spectra of ocean seismic reflectors agrees with Garrett-Munk model spectra of internal wave displacements [*Holbrook and Fer*, 2005; *Krahmann et al.*, 2008]. All these observations have sparked interest in the technique within the physical oceanographic community.

[4] Although it is now clear that the ocean's seismic reflectivity is due to acoustic impedance contrasts associated with oceanic fine structure, there is an ongoing debate concerning the relative contribution of the water's physical properties to this reflectivity, key to understand what is the information of oceanographic interest that can be extracted from seismic data. Most estimations made to date are based on waveform analysis of isolated XBT (expandable bathythermograph)-derived hydrographic profiles, suggesting that the contribution of sound speed (v) is the major factor as compared with that of density (ρ) [e.g., *Nandi et al.*, 2004; *Krahmann et al.*, 2008], and changes in temperature dominate in turn those of salinity. A first attempt to calculate this relative contribution was made by *Ruddick et al.* [2009], who used the expressions of *Lavery et al.* [2003] for the partial derivatives of v and ρ with respect to temperature (T) and salinity (S) at a given T (12°C), S (35.4) and pressure (P, 1000 dbar) to determine the relative contribution of T and S to impedance contrasts. For these particular T, S, P values, they found that the contribution of T is almost five-fold that of S. There has however been no formal attempt to date to generalize these conclusions by calculating the complete expressions of the partial derivatives, which significantly change with T, S, and P, and apply them to a real oceanographic data set in order to determine

[1]Unitat de Tecnologia Marina, Consejo Superior de Investigaciones Científicas, Barcelona, Spain.
[2]Institut of Earth Sciences "Jaume Almera," Consejo Superior de Investigaciones Científicas, Barcelona, Spain.
[3]Institut de Ciencies del Mar, Consejo Superior de Investigaciones Científicas, Barcelona, Spain.

0094-8276/09/2009GL040187$05.00

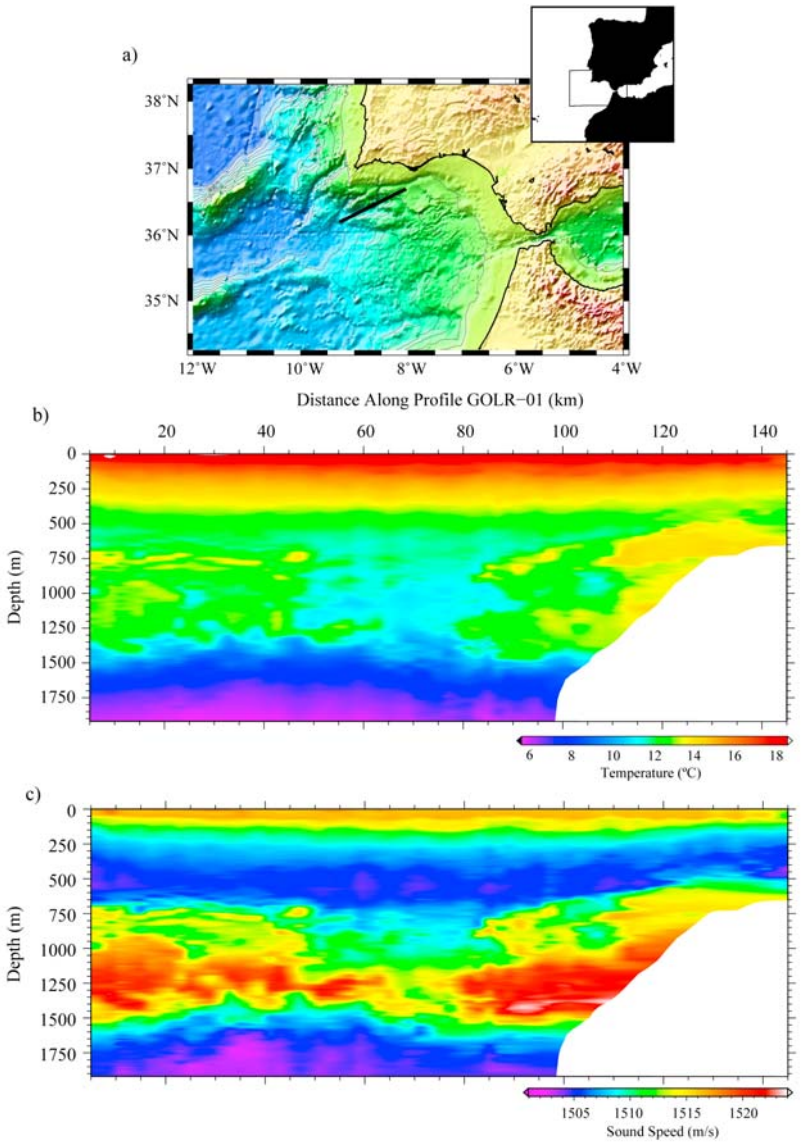

Figure 1. (a) Location map of the D318B-GO survey study zone. The thick line indicates the location of the coincident seismic and hydrographic profile GO-LR-01. (b) 2-D temperature-depth map obtained from XBT and CTD data acquired during the D318-GO survey along the profile GO-LR-01. The data have been interpolated for imaging purposes using the minimum curvature surface algorithm of *Smith and Wessel* [1990]. (c) 2-D sound speed-depth map along the same profile obtained using *Chen and Millero*'s [1976] empirical relationship. The temperature is that measured with XBT and CTD (Figure 2a) and the salinity has been inferred based on CTD data.

the actual range of variation of the different contributions. This is what we do in this work: we first calculate the partial derivatives of sound speed and density with respect to T and S based on UNESCO formulas [*Chen and Millero*, 1976; *Millero et al.*, 1980], then incorporate the expressions into linearized Zoeppritz equations of reflection coefficients [*Aki and Richards*, 1980], and finally apply the resulting expressions to real, high-resolution, T and S data recently acquired in the Gulf of Cadiz [*Hobbs et al.*, 2007].

2. Data

[5] The hydrographic data used in this study were collected in April, 2007 during the coincident seismic and oceanographic NERC-318B survey made on-board British RRS Discovery and German FS Poseidon in the SW Iberian margin, as part of the EU project "Geophysical Oceanography: A new tool to understand the thermal structure and dynamics of oceans (GO)" [*Hobbs et al.*, 2007]. During the survey, 1200 km of MCS lines and coincident, high-resolution XBT and XCTD stations were acquired by RRS Discovery, while simultaneous XBT and CTD casts were made by FS Poseidon [*Hobbs et al.*, 2007]. XBT-profiles were quality controlled, and anomalous data were removed. Depth was corrected according to the fall-rate equations of *Boyd and Linzell* [1993] for Sippican T-5. The error in depth with respect to adjoining CTDs was typically less than 5 m over the 1800 m depth range. From among the available hydrographic data, we have selected those acquired along profile GO-LR-01 (Figure 1a). It is 145 km-long and runs

NE–SW offshore Portimao crossing the core of the Mediterranean Undercurrent, which transports Mediterranean water (MW) west from the Strait of Gibraltar as it sinks along the continental slope of the Iberian margin. Figure 1b shows the 2D temperature map obtained by merging together all the XBT and CTD data (49 and 5 profiles, respectively) acquired along line GO-LR-01. The mean separation between adjoining casts is ~2.5 km.

[6] Simultaneous temperature and salinity values, measured during the whole GO survey (40 in total) have been used to assign S-values to the XBT-derived T, depth (z) pairs. The corresponding S-values have been calculated following a statistical approach that consisted of: 1) computing all the CTD-measured T, z (and S) values that fall within ΔT, Δz of each XBT-measured T, z pair; and 2) assigning S to XBT-measured T, z pairs as a Gaussian-weighted average of all the selected CTD-measured S values. We have tested different values for ΔT, Δz as well as for the Gaussian's standard deviations σ_T and σ_z, and found that a set of parameters giving a good compromise between data accuracy and data density are $\Delta T = 0.02°C$, $\sigma_T = 0.002°C$, and $\Delta z = 5$ m, $\sigma_z = 0.5$ m. The accuracy was evaluated by comparing the salinity obtained with that measured with a CTD cast made during the GO survey but not used in the assignment. The mean difference obtained is less than 1.5×10^{-3}.

[7] The locally measured temperature and pressure values, together with the statistically inferred salinities, have been used to calculate density and sound speed. Density has been computed using the empirical UNESCO's International Equation of Seawater from 1980 (EOS80), which is claimed to be valid for S = 0–42, T = −2–40°C, and P = 0–1000 bars. Details on the fitting procedure and the different terms of the polynomial regressions are available from *Millero et al.* [1980]. Sound speed (Figure 1c) has been calculated using the empirical relationship of *Chen and Millero* [1976], which is also compliant with the practical salinity scale and is the one giving the best agreement with values computed from EOS80. The temperature and sound speed maps of Figures 1b and 1c clearly show the presence of the relatively warm, salty and fast MW mass between 700 m and 1500 m depth along the whole profile.

3. Method

[8] The strategy to estimate the relative contribution of sound speed vs. density and temperature vs. salinity on reflectivity at the seismic source wavelength consists of three main steps, namely (1) the computation of the T and S partial derivatives using the UNESCO formulas for density and sound speed on a scale one order of magnitude smaller to the source wavelength, (2) the incorporation of the resulting expressions into the Zoeppritz equations for the reflection coefficients, (3) the calculation of the relative significance of the different properties to the reflection coefficients along the hydrographic profile shown in Figure 1a, and (4) the convolution with the source wavelet.

[9] There are many works dealing with the Zoeppritz equations for the transmission/reflection coefficients of plane waves in layered media. Since Zoeppritz equations are highly nonlinear with respect to speed and density, many approximations have been attempted in order to linearize them. Here we follow that proposed by *Aki and Richards* [1980], which is suitable for elastic media having weak property contrasts. When the two adjoining layers have similar properties; that is, if there is, over a vertical distance Δz, a jump in magnitudes of $\Delta\rho = \rho_2 - \rho_1$, $\Delta\alpha = \alpha_2 - \alpha_1$ and $\Delta\beta = \beta_2 - \beta_1$ that is very small so the ratios $\Delta\rho/\rho$, $\Delta\alpha/\alpha$, and $\Delta\beta/\beta$ (where ρ, α, and β are the mean value of density, compressional, and shear waves speed of the two media) are much lower than unity, then transmission will largely dominate reflection (i.e., the reflection coefficient, R, will be close to zero). In this case it makes sense to derive the first-order effect of small jumps in density and sound speed because the resulting expressions are remarkably accurate [e.g., *Aki and Richards*, 1980] and, at the same time, give good insight into the separate contributions made by $\Delta\alpha$, $\Delta\beta$ and $\Delta\rho$. For acoustic media such as the water column, where $\beta = 0$, $\Delta\alpha/\alpha$ is on the order of 10^{-3}–10^{-4}, and $\Delta\rho/\rho$ is even smaller, the resulting expression for the reflection coefficient depend on the angle of incidence (i) and the density and sound speed (v) contrasts only. It is given as $R = R_v + R_\rho$, where

$$R_v = \frac{\Delta v}{2v \cdot \cos^2 i} \tag{1}$$

and

$$R_\rho = \frac{\Delta\rho}{2\rho} \tag{2}$$

correspond respectively to the contribution to R made by Δv and $\Delta\rho$. The relative contribution of $\Delta\rho$ and Δv to R is then calculated as R_v/R and R_ρ/R.

[10] Without considering the effect of pressure variations, $\Delta\rho$ and Δv can be expressed as a function of the temperature and salinity variations, ΔT and ΔS, as

$$\Delta\rho_{TS} \cong \frac{\partial\rho}{\partial T}\Delta T + \frac{\partial\rho}{\partial S}\Delta S \tag{3}$$

and

$$\Delta v_{TS} \cong \frac{\partial v}{\partial T}\Delta T + \frac{\partial v}{\partial S}\Delta S \tag{4}$$

where $\partial\rho/\partial$T, $\partial\rho/\partial$S, ∂v/∂T, ∂v/∂S are the partial derivatives of density and sound speed with respect to T and S. Combining (1), (2), (3) and (4) we obtain $R_{TS} = R_T + R_S$, where

$$R_T = \frac{\Delta T}{2} \cdot \left[\frac{\partial\rho/\partial T}{\rho} + \frac{\partial v/\partial T}{v \cdot \cos^2 i}\right] \tag{5}$$

and

$$R_S = \frac{\Delta S}{2} \cdot \left[\frac{\partial\rho/\partial S}{\rho} + \frac{\partial v/\partial S}{v \cdot \cos^2 i}\right] \tag{6}$$

correspond to the contribution to the reflection coefficient made by ΔT and ΔS, respectively. We can then estimate the relative contribution of ΔT and ΔS as R_T/R_{TS} and R_S/R_{TS} (R_T/R and R_S/R from here on).

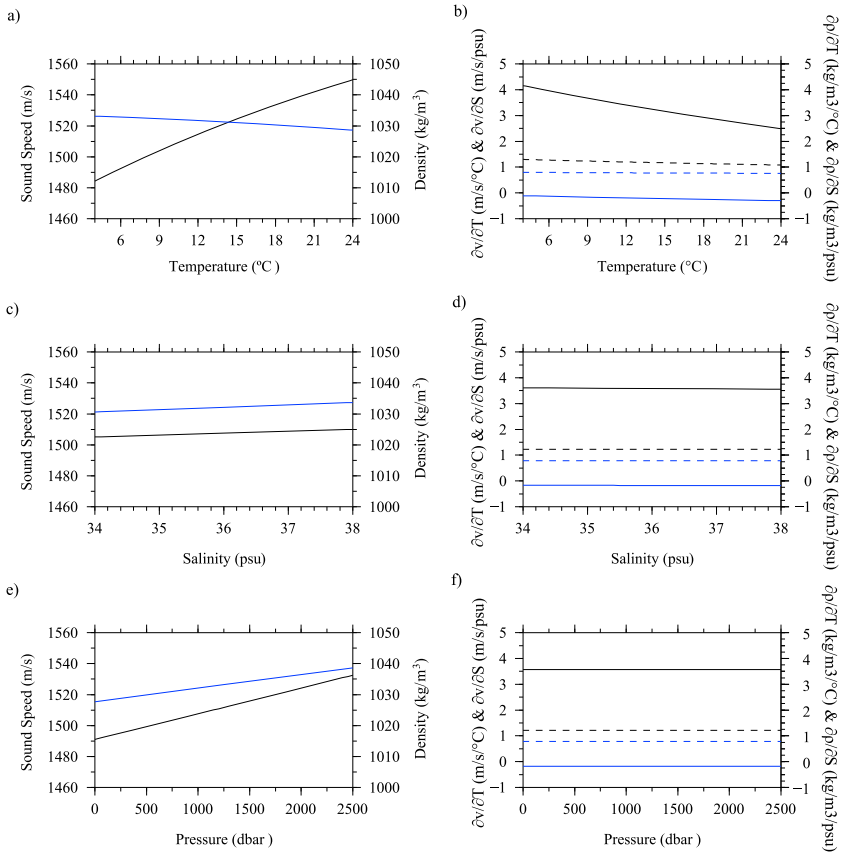

Figure 2. Diagrams of physical properties and their T, S partial derivatives obtained using the EOS80 expressions for sound speed and density. Sound speed (black line) and density (blue line) vs. (a) temperature, (c) salinity and (e) pressure. $\partial v/\partial T$ (solid black line), $\partial v/\partial S$ (dashed black line), $\partial\rho/\partial T$ (solid blue line), $\partial\rho/\partial S$ (dashed blue line) vs. (b) temperature, (d) salinity and (f) pressure.

[11] Figure 2 shows diagrams of v, ρ and their T and S partial derivatives as a function of T, S and P calculated with the EOS80 relationships referred to above. Note that sound speed increases with increasing T, S and P, whereas density increases with increasing S and P but decreases with increasing T. Regarding the partial derivatives, $\partial v/\partial T$ decreases substantially with increasing T and very slightly with increasing S, whereas $\partial\rho/\partial T$ decreases with increasing T and S. Both $\partial v/\partial S$ and $\partial\rho/\partial S$ decrease slightly with increasing T and hardly vary with S.

[12] R_v, R_ρ and R_T, R_S have been computed for all XBTs using the v, ρ, $\partial v/\partial T$, $\partial v/\partial S$, $\partial\rho/\partial T$, $\partial\rho/\partial S$ values obtained along the whole profile and calculating Δv, $\Delta\rho$, ΔT, ΔS as a sample-by-sample difference from top to bottom of each profile, which corresponds to a vertical distance of Δz = 65 cm. The resulting values are then convolved with a Ricker wavelet of 50 Hz, adequate to characterize fine structure. Given that temperature and salinity are highly correlated, the relative T, S contribution is basically independent of the vertical smoothing made in the range of 25–50 Hz.

4. Discussion of Results

[13] The results obtained for R_v/R, R_ρ/R and R_T/R, R_S/R along profile GO-LR-01, expressed as a percentage of the relative contribution for normal incidence after convolution with the source wavelet, are shown in Figure 3. It is clear that the mean contribution to the water reflectivity comes, as expected, from Δv through ΔT, in agreement with previous works confirming that the influence of Δv and ΔT is major compared to $\Delta\rho$ and ΔS [e.g., *Nandi et al.*, 2004; *Krahmann et al.*, 2008]. On one hand, the mean value of R_v/R along GO-LR-01 is 90%, whereas R_ρ/R accounts for the remaining 10%. The standard deviation of both R_v and R_ρ is 11%. These values agree with those estimated by *Krahmann et al.* [2008] based on waveform analysis of XBT data in the same area (~90%), and are smaller to those proposed by *Ruddick et al.* [2009] using the expressions derived by *Lavery et al.* [2003] for scattering of high-frequency acoustic waves at constant T, P and S (~99%). In the case of non-normal incidence, the contribution of Δv increases by a factor of $1/\cos^2 i$ and that of $\Delta\rho$ remains constant. On the other hand, the mean value of R_T/R is 80%, while that of R_S/R is 20%, with a standard deviation of 12%. R_S/R is somewhat larger than that estimated by *Ruddick et al.* [2009] (17%). Overall these results illustrate that while R_ρ/R is, on average, one-to-two orders of magnitude smaller than R_v/R, and it could thus be safely neglected when inferring sound speed from seismic data, R_S/R is only four-fold weaker than R_T/R, so it should not be ignored. Given that $\partial v/\partial T$ is two- to four-fold larger than $\partial v/\partial S$, the influence of non-normal incidence to R_S/R is smaller than to R_T/R, so the relative contribution of S decreases with

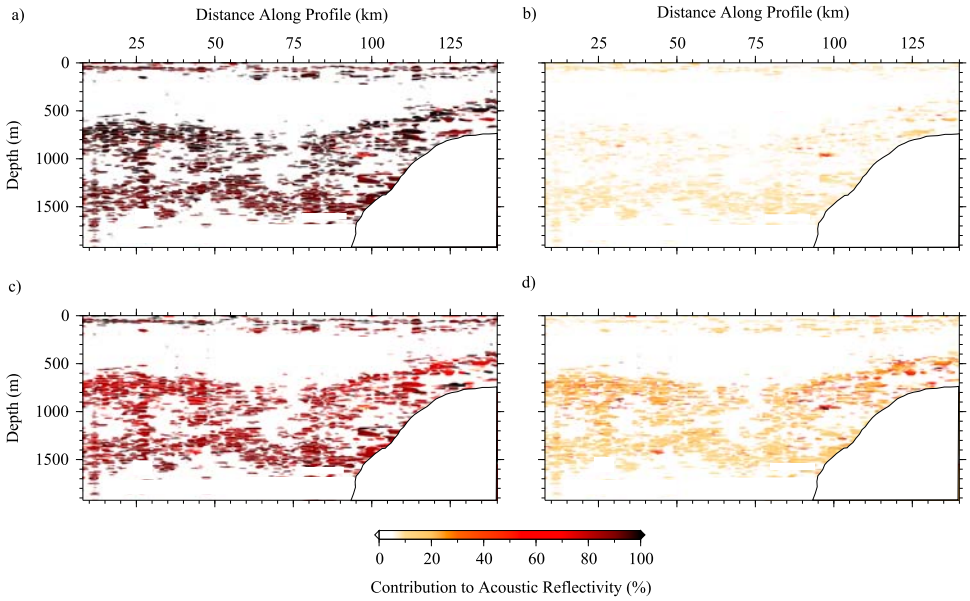

Figure 3. 2-D maps representing the percentage of the partial contribution of (a) sound speed (R_v/R) vs. (b) density (R_ρ/R), and (c) temperature (R_T/R) vs. (d) salinity (R_S/R) to the reflectivity of the water column along profile GO-LR-01 (Figure 1). These maps have been obtained convolving the reflection coefficients with a 50 Hz Ricker wavelet. In order to concentrate the information on the brightest reflectors, only points exceeding the mean R value are displayed. As in Figure 1, data interpolation has been made using the minimum curvature surface algorithm of *Smith and Wessel* [1990].

increasing i. It is interesting to note, however, that the relative contribution of the different properties strongly varies within the water column along the whole profile (Figure 3). The highest R_S/R (and lowest R_T/R) is systematically found at the top of the MW (i.e., 700–900 m deep), whereas the lowest R_S/R (and highest R_T/R) is found at the bottom of the MW (i.e., 1200–1400 m deep). R_S/R is 27% on average, and locally achieves 35–40% at the top of the MW. At the bottom of the MW, R_S/R is 16% on average. The contribution of salinity to seismic reflectivity is therefore considerably larger at the top than at the bottom of the MW. This large R_T/R, R_S/R variability prevents one from univocally determining T and S based on seismic data alone. R_v/R and R_ρ/R show a trend similar to that of R_S/R and R_T/R, in being that the mean R_ρ/R value is two-times larger at the bottom (12%) than at the top (6%) of the MW.

[14] It is noteworthy that the regions showing the largest contribution of salinity contrasts to reflectivity are found in areas of unstable temperature gradients, with dominant thermal flux and prone to mixing by diffusive convection such as the top of the MW, whereas the smallest salinity (and largest density) contribution occurs in places of unstable salt gradients, presumed to be dominated by salt fingering, such as the bottom of the MW [*Schmitt*, 1994].

5. Conclusions

[15] Marine MCS systems are well-adapted to image oceanic fine-structure. The strength of the reflectivity associated with a given water boundary layer is proportional to the acoustic impedance contrast between the two neighbouring water masses, which is in turn a function of sound speed and density (i.e., temperature and salinity) changes across the layer at the seismic source frequency bandwidth. The main contribution to seismic reflectivity is that of sound speed variations, which is, on average, one-to-two-orders of magnitude larger than that of density (90–95% vs. 5–10%). Likewise, temperature contrasts account on average for ~80% of the reflectivity, and salinity for the remaining ~20%. The partial contribution of the different properties is however highly variable. Interestingly, salinity contribution can be as high as 40% in the top of MW features, but only around 15% in other regions such as at the base of the MW. This variability makes it virtually impossible to derive temperature and salinity from seismic data alone. In the region under study, the areas showing the largest salinity contribution correspond to areas prone to diffusive convection such as at the top of MW features, whereas those showing the smallest salinity contribution are those prone to salt fingering.

[16] **Acknowledgments.** This work is part of the EU-FP6 funded GO project (NEST-2003-1 FP6015603), and the data set used here was acquired in the framework of this project. It has also been supported by the Consejo Superior de Investigaciones Científicas (CSIC) through GEOCEAN PIF Project 200530f081. CSIC is also funding the second author's work by means of a JaeDoc contract. Constructive reviews made by R. Hobbs and two anonymous reviewers are acknowledged.

References

Aki, K., and P. G. Richards (1980), *Quantitative Seismology: Theory and Methods*, W. H. Freeman, San Francisco, Calif.

Biescas, B., V. Sallarès, J. L. Pelegrí, F. Machín, R. Carbonell, G. Buffett, J. J. Dañobeitia, and A. Calahorrano (2008), Imaging meddy fine structure using multichannel seismic data, *Geophys. Res. Lett.*, *35*, L11609, doi:10.1029/2008GL033971.

Boyd, J. D., and R. S. Linzell (1993), The temperature and depth accuracy of Sippican T-5 XBTs, *J. Atmos. Oceanic Technol.*, *10*, 128–136, doi:10.1175/1520-0426(1993)010<0128:TTADAO>2.0.CO;2.

Buffett, G., B. Biescas, J. L. Pelegrí, F. Machín, V. Sallarès, R. Carbonell, D. Klaeschen, and R. Hobbs (2009), Seismic reflection along the path of the Mediterranean Undercurrent, *Cont. Shelf Res.*, *29*, 1848–1860, doi:10.1016/j.csr.2009.05.017.

Chen, C. T., and F. J. Millero (1976), Speed of sound in seawater at high pressures, *J. Acoust. Soc. Am.*, *60*, 1270–1273, doi:10.1121/1.381240.

Hobbs, R., et al. (2007), GO—Geophysical Oceanography: A new tool to understand the thermal structure and dynamics of oceans, *D318 Cruise Rep.*, Durham Univ., Durham, U. K. (Available at http://www.dur.ac.uk/eu.go/cruise/report.html)

Holbrook, W. S., and I. Fer (2005), Ocean internal wave spectra inferred from seismic reflection transects, *Geophys. Res. Lett.*, *32*, L15604, doi:10.1029/2005GL023733.

Holbrook, W. S., P. Paramo, S. Pearse, and R. W. Schmitt (2003), Thermohaline fine structure in an oceanographic front from seismic reflection profiling, *Science*, *301*, 821–824, doi:10.1126/science.1085116.

Krahmann, G., P. Brandt, D. Klaeschen, and T. Reston (2008), Mid-depth internal wave energy off the Iberian Peninsula estimated from seismic reflection data, *J. Geophys. Res.*, *113*, C12016, doi:10.1029/2007JC004678.

Lavery, A., R. W. Schmitt, and T. K. Stanton (2003), High-frequency acoustic scattering from turbulent oceanic microstructure: The importance of density fluctuations, *J. Acoust. Soc. Am.*, *114*, 2685–2697.

Millero, F. J., C. T. Chen, A. Bradshaw, and K. Schleicher (1980), A new high pressure equation of state for seawater, *Deep Sea Res., Part A*, *27*, 255–264, doi:10.1016/0198-0149(80)90016-3.

Nakamura, Y., T. Noguchi, T. Tsuji, S. Itoh, H. Niino, and T. Matsuoka (2006), Simultaneous seismic reflection and physical oceanographic observations of oceanic fine structure in the Kuroshio extension front, *Geophys. Res. Lett.*, *33*, L23605, doi:10.1029/2006GL027437.

Nandi, P., S. Holbrook, S. Pearse, P. Paramo, and R. Schmitt (2004), Seismic reflection imaging of water mass boundaries in the Norwegian Sea, *Geophys. Res. Lett.*, *31*, L23311, doi:10.1029/2004GL021325.

Ruddick, B., and A. Gargett (2003), Oceanic double-diffusion: Introduction, *Prog. Oceanogr.*, *56*, 381–393, doi:10.1016/S0079-6611(03)00024-7.

Ruddick, B., H. Song, C. Dong, and L. Pinheiro (2009), Water column seismic images as maps of temperature gradient, *Oceanography*, *22*, 192–205.

Schmitt, R. W. (1994), Double diffusion in oceanography, *Annu. Rev. Fluid Mech.*, *26*, 255–285, doi:10.1146/annurev.fl.26.010194.001351.

Sheriff, R. E., and L. P. Geldart (1995), *Exploration Seismology*, 2nd ed., 592 pp., Cambridge Univ. Press, Cambridge, U. K.

Smith, W. H. F., and P. Wessel (1990), Gridding with continuous curvature splines in tension, *Geophysics*, *55*, 293–305, doi:10.1190/1.1442837.

Tsuji, T., T. Noguchi, H. Niino, T. Matsuoka, Y. Nakamura, H. Tokuyama, S. Kuramoto, and N. Bangs (2005), Two-dimensional mapping of fine structures in the Kuroshio Current using seismic reflection data, *Geophys. Res. Lett.*, *32*, L14609, doi:10.1029/2005GL023095.

Widess, M. (1973), How thin is a thin bed?, *Geophysics*, *38*, 1176–1180, doi:10.1190/1.1440403.

B. Biescas, J. J. Dañobeitia, and V. Sallarès, Unitat de Tecnologia Marina, Consejo Superior de Investigaciones Científicas, Passeig Marítim de la Barceloneta, 37-49, E-08003 Barcelona, Spain. (vsallares@cmima.csic.es)

G. Buffett and R. Carbonell, Institut of Earth Sciences "Jaume Almera," Consejo Superior de Investigaciones Científicas, Lluis Solé i Sabarís, s/n, E-08028 Barcelona, Spain.

J. L. Pelegrí, Institut de Ciencies del Mar, Consejo Superior de Investigaciones Científicas, Passeig Marítim de la Barceloneta, 37-49, E-08003 Barcelona, Spain.